

Opinion formation models on a gradient

Michael T. Gastner,^{1,2,3} Nikolitsa Markou,⁴ Gunnar Pruessner,² and Moez Draief⁴

¹*Department of Engineering Mathematics, University of Bristol, Merchant Venturers Building, Woodland Road, Bristol BS8 1UB, UK*

²*Department of Mathematics, Imperial College London, South Kensington Campus, London SW7 2AZ, UK*

³*Institute of Technical Physics and Materials Science, Research Centre for Natural Sciences, Hungarian Academy of Sciences, P.O. Box 49, H-1525 Budapest, Hungary*

⁴*Department of Electrical and Electronic Engineering, Imperial College London, South Kensington Campus, London SW7 2AZ, UK*

Statistical physicists have become interested in models of collective social behavior such as opinion formation, where individuals change their inherently preferred opinion if their friends disagree. Real preferences often depend on regional cultural differences, which we model here as a spatial gradient g in the initial opinion. The gradient does not only add reality to the model. It can also reveal that opinion clusters in two dimensions are typically in the standard (i.e. independent) percolation universality class, thus settling a recent controversy about a non-consensus model. However, using analytical and numerical tools, we also present a model where the width of the transition between opinions scales $\propto g^{-1/4}$, not $\propto g^{-4/7}$ as in independent percolation, and the cluster size distribution is consistent with first-order percolation.

Introduction

Disagreement between neighbors costs energy, in human societies as well as in ferromagnetic spin interactions. Because of this similarity, statistical physicists have recently shown great interest in models of opinion formation (e.g. [1–6], see [7, 8] for literature reviews). Individual actors in a population are regarded as nodes in a network and their opinions represent political affiliations, religions or consumer choices (Microsoft WindowsTM vs. UN*X, Blu-rayTM vs. HD-DVD, etc.). The nodes influence each other’s opinions along the edges in the network according to rules specific to the model in question. Rules that allow a critical mass of like-minded peers to persuade a disagreeing individual have recently found support in behavioral experiments [9]. The resulting opinion dynamics has been linked to election outcomes [10, 11] and innovation diffusion [12, 13], suggesting lessons for political campaigns [14] and advertisement [15].

Many opinion formation models embedded in two-dimensional space have only one stable solution, namely complete consensus [3, 5, 16], in particular when they implement deterministic rules. In reality, however, deterministic social behavior and perfect agreement are rare [17] – at least one small village of indomitable Gauls always holds out against the Romans. Some models thus allow clusters of a minority opinion to persist even if entirely surrounded by the opposite opinion [18, 19]. In this case, percolation theory provides the tools to analyze the geometry of the minority clusters [19, 20]. However, the results [19, 21] have been subject to some controversy because long-range correlations, thought to be responsible for deviations from independent percolation, are expected to require a long time to develop from an uncorrelated initial state [22]. Clearly, interactions generate complex correlations that can obscure the familiar scaling behavior of independent percolation. However, as

illustrated in the present work, one must exercise great care before concluding that a given interaction spoils the (asymptotic) scaling of independent percolation.

In this article we tackle the open question: can opinion dynamics, with or without a stochastic element, fundamentally alter percolation properties such as the clusters’ fractal dimensions or the cluster size distribution? We show that in many cases we retrieve the scaling laws of independent percolation. Moreover, we also give one example where a slight change of the dynamic rules leads to a radically different scaling behavior.

Methods

We focus on models where the nodes are placed on a square lattice with edges linking them to their four nearest neighbors. Each node holds one of two possible opinions: “black” or “white”. Initially, the probability to be black is independent at all sites and given by

$$p(x) = gx + p_c, \quad x \in [-p_c/g, (1 - p_c)/g], \quad (1)$$

where x is the node’s horizontal position and $g \in \mathbb{R}^+$ a constant gradient. (We set the intercept p_c equal to the percolation threshold for later convenience.) We interpret $p(x)$ as the innate propensity to hold the black opinion at the beginning as well as during the evolution of the opinions. Thus, nodes on the far left and far right of the lattice are likely to have opposite opinions. Some previous spatial models have included heterogeneous agents [23–25], but no gradient. In contrast, election results in various countries exhibit clear, smooth gradients, especially between progressive urban and conservative rural areas [26–28]. Our model resembles such a “culture war” fought on a gradient.

Including a non-zero gradient in the numerical simulations also has advantages for studying percolation prop-

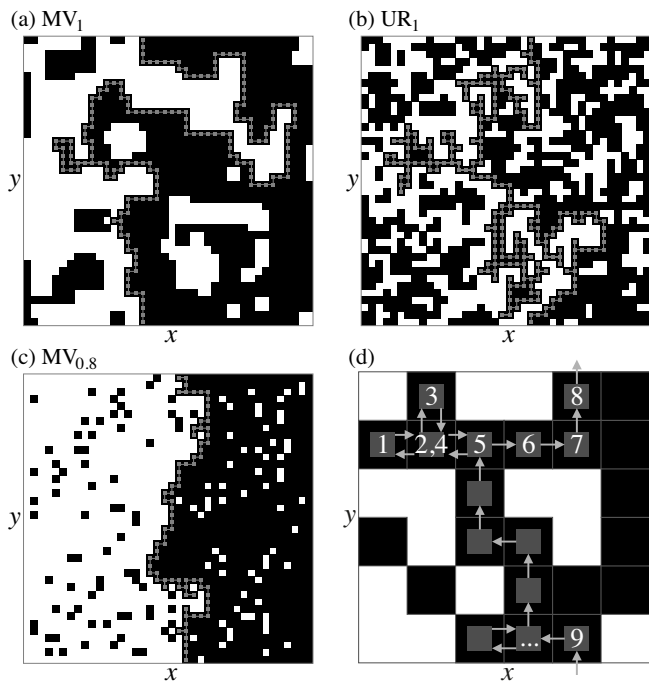


FIG. 1: **Opinion distributions and percolation hull.** We show typical steady-state opinion distributions for $g = 5 \times 10^{-3}$ and (a) MV_1 , (b) UR_1 , (c) $MV_{0.8}$. The two opposing opinions are shown as black and white squares. The sites marked by gray squares form the spanning cluster's hull. (d) Illustration how the hull can be parameterized by a left-turning walk [33].

erties [29]. As opposed to running many individual simulations for a range of different values of p , a gradient model allows us to analyze, in a single simulation, clusters for a whole interval of p rather than a single fixed value.

In the present work we consider opinion formation according to the following local rules.

- Majority vote (MV): the node follows the majority opinion of its four nearest neighbors. If both opinions are equally represented, no opinion change occurs.
- Unanimity rule (UR): the node changes its current opinion if and only if all of its nearest neighbors hold the opposite opinion [30].
- Independent percolation (IP): the node keeps its current opinion irrespective of the surrounding opinions.

When a node is updated, it follows the local rule with probability q . Otherwise it independently chooses a random opinion according to Eq. 1, so that $1 - q$ is the level of noise entering the dynamics. Notably, Eq. 1 is the only way for the local prevalence of a certain opinion and thus the gradient to enter into the dynamics of the system. At

$q = 1$ the evolution is affected by the presence of the gradient only through the initial condition. At $q < 1$ the random updates during the evolution exhibit the innate propensity gradient towards one or the other opinion by allowing agents to revert to their original opinion even if it contradicts the local majority.

All nodes simultaneously update their opinion at each time step, but other choices such as random sequential updates do not change our findings noticeably. The latter may have the more immediate social interpretation as an ongoing opinion formation with agents re-considering choices with a fixed rate, but simultaneous updates are, surprisingly, slightly more accessible analytically. For a fixed value of q , we abbreviate the models by MV_q or UR_q , respectively. We do not need a subscript q for IP because, regardless of the value of q , any snapshot of the lattice looks statistically alike, depending only on the parameters p_c and g in Eq. 1.

Once the model reaches the steady state, we study the geometric properties of the clusters formed. On the left of Fig. 1(a)-(c), the black clusters form small isolated islands, whereas on the right a single large black cluster spans from top to bottom [31]. This percolation transition can be characterized by the hull of the spanning cluster [32], defined as the following left-turning walk [33, 34]. We start the walk at a site with minimal x -coordinate in the black spanning cluster and face towards the right (Fig. 1d). First we attempt to turn to the neighbor on our left, but step in this direction only if we reach a black site. Otherwise, we try to move forward, then to the right, and finally backward until we have discovered the first black neighbor. If we iterate this procedure and apply periodic boundary conditions in the y -direction, the hull has visited the entire front of the spanning cluster when it returns to the starting position.

Steady-state hull width and length

If $q = 1$, the dynamics is deterministic and the only source of randomness lies in the initial assignment of opinions. In this special case, MV_1 is identical to the non-consensus opinion model of Ref. [19], where it was already noted that a small fraction of the nodes – in our simulations 1.2% on average at $p_c = 0.50643(1)$ – keeps switching opinions with period 2. When all other nodes have stopped changing opinions, we will consider MV_1 to have reached its steady state. The convergence is quick: a non-periodic node freezes after a mean of only 0.8 time steps. In UR_1 , oscillatory opinions can occur only if the initial opinions form a perfect checkerboard pattern. Because the gradient pins the left (right) edge to be entirely white (black), a checkerboard pattern is impossible. Hence, every node reaches a stationary opinion, on average after just 0.06 updates at $p_c = 0.549199(5)$. For IP, percolation occurs, as in zero-gradient percolation, at $p_c = 0.59274(1)$ [35].

If $q < 1$, the opinions in MV_q and UR_q never freeze,

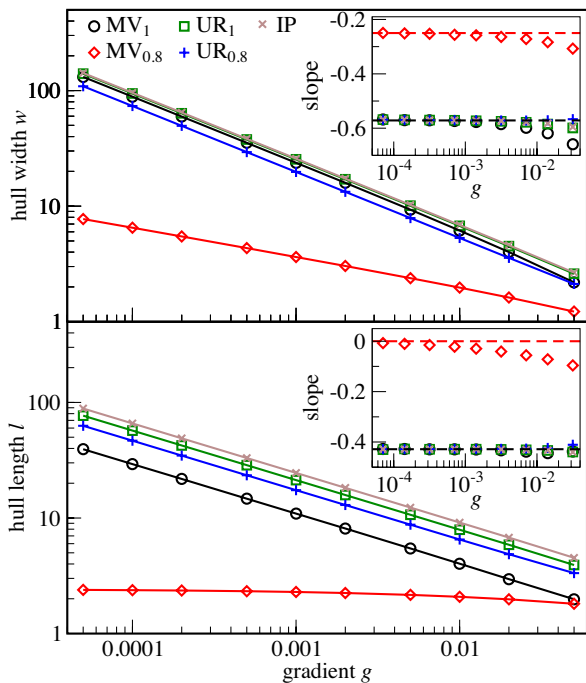


FIG. 2: Mean hull width and length determined numerically as a function of the gradient. Insets: slope in doubly-logarithmic scales (i.e. $d \log(w)/d \log(g)$ in upper, $d \log(l)/d \log(g)$ in lower panel). Dashed lines indicate the limiting slopes for $g \rightarrow 0^+$ which follow from scaling analysis (see text): $-4/7$ and $-1/4$ in the upper, $-3/7$ and 0 in the lower panel. Error bars are smaller than the symbol sizes.

but, after a transient, the stochastic time series of black occupancy in any column x becomes stationary. All measurements for $q < 1$ presented here were made at $q = 0.8$ in this steady state. A visual comparison between Fig. 1(a)-(c) suggests a qualitative difference between MV_1 and UR_1 on the one hand and $MV_{0.8}$ on the other hand. In the latter case, the spanning cluster appears significantly more compact and the hull, which is centered at $p_c = 0.5000(4)$, much straighter. So, counterintuitively, the stochastic dynamics of $MV_{0.8}$ anneals rather than roughens the surface compared to MV_1 and UR_1 .

We can quantify this observation by computing the hull’s width w and length l . If the hull consists of the walk $(x_1, y_1), \dots, (x_l, y_l)$, we define

$$w = \sqrt{\frac{\sum_i x_i^2}{l} - \left(\frac{\sum_i x_i}{l}\right)^2}. \quad (2)$$

As the numerical results in Fig. 2 show, the width and length for all models scale as power laws $w \propto g^{-a}$ and $l \propto g^{-b}$ in the limit $g \rightarrow 0^+$. With only one exception among all investigated cases, the results are consistent with $a = 4/7$ and $b = 3/7$, the exact exponents of independent gradient percolation [36]. We also retrieve the correlation length critical exponent ν of standard perco-

lation via the formula $\nu = a/(1-a) = (1-b)/b = 4/3$ [31]. The notable exception is $MV_{0.8}$ with $a = 0.250(4)$ and $b = 0.0074(1)$, based on numerics for $g = 10^{-4}$ and $g = 5 \times 10^{-5}$. Studying the dependence of b on g systematically suggests $b \rightarrow 0$ for $g \rightarrow 0$, while a stays close to $1/4$. In fact, the analytical results presented below indicate that $a = 1/4$ and $b = 0$. In independent percolation, $a \neq 4/7$ can arise only if the probability to be black increases nonlinearly at the percolation threshold [37]. However, in that case the ratio b/a must still equal $3/4$ which is not true for $MV_{0.8}$ so that we must look elsewhere for an explanation.

We will briefly summarize why a equals $1/4$ for MV_q if q is close to, but not equal to 1 . For details we refer to Appendices 1–3. We make two approximations. (1) The hull can be treated as a single-valued function of y so that we can parameterize the hull at time t as a function $h(t, y)$. (2) In $MV_{0.8}$, as opposed to UR_q and IP , we observe only few isolated minority nodes, which motivates a “solid-on-solid” approximation: we neglect that there is a small number of black (white) sites to the left (right) of $h(t, y)$. With the notation $r = 1 - q$, the only transition probabilities for $h(t, y)$ up to terms of order $O(r^2)$ are (see Appendix 1)

$$\Pr[h \rightarrow h - 1 + K_y] = r \left[\frac{1}{2} + g \left(h - \frac{1}{2} + K_y \right) \right], \quad (3)$$

$$\Pr[h \rightarrow h + K_y] = 1 + r(g - 1), \quad (4)$$

$$\Pr[h \rightarrow h + 1 + K_y] = r \left[\frac{1}{2} - g \left(h + \frac{1}{2} + K_y \right) \right], \quad (5)$$

where $K_y = +1$ if $h(t, y)$ is a strict local minimum in y , $K_y = -1$ for a maximum, and $K_y = 0$ otherwise. In the continuum limit [38], the leading terms in the evolution of the hull are (see Appendix 2)

$$\frac{\partial h}{\partial t} = D \frac{\partial^2 h}{\partial y^2} - Egh + F\eta(t, y), \quad (6)$$

where D, E, F are independent of g and η is white noise with mean zero and covariance $\langle \eta(t, y)\eta(t', y') \rangle = \delta(t - t')\delta(y - y')$. Equation 6 is the Edwards-Wilkinson equation [39] with an Ornstein-Uhlenbeck restoring force [40, 41] and can be integrated (see Appendix 3) to obtain the continuum limit of Eq. 2,

$$w^2 = \lim_{t \rightarrow \infty} \langle \overline{h(t)^2} - \overline{h(t)}^2 \rangle = \frac{F^2}{4\sqrt{DEg}}, \quad (7)$$

where the angle brackets denote the ensemble average and the overlines symbolize spatial averages. Thus, we obtain $w \propto g^{-1/4}$ consistent with the numerical results for $MV_{0.8}$. Although we have here derived the scaling law only for the MV model, numerical evidence suggests that $a = 1/4$ is valid for a broader class of gradient models. In Ref. [42], a numerical fit for a spatial birth-death process on a gradient also yields $a = 0.26(1)$.

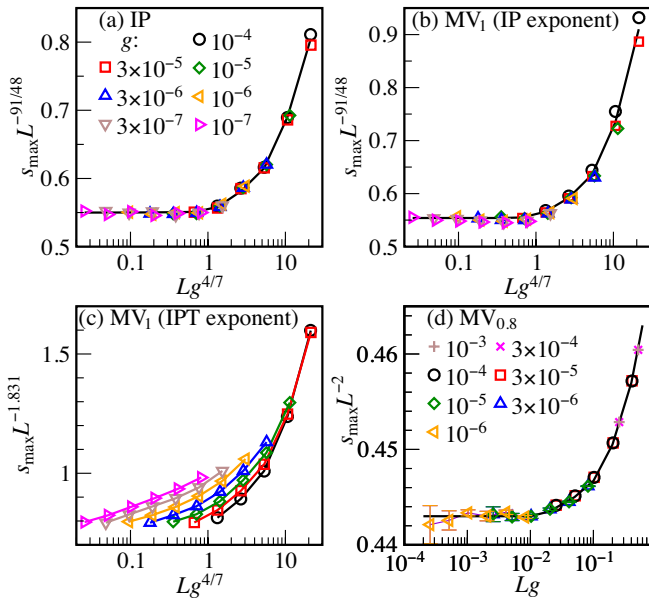


FIG. 3: **Fractal dimensions.** For the correct exponents d_f and c , $s_{\max} L^{-d_f}$ as a function of Lg^c should collapse on a single curve with slope zero for $Lg^c \rightarrow 0$. For (a) IP and (b) MV₁, $d_f = 91/48$ is the same as the fractal dimension of standard percolation. (c) Replacing d_f with the value 1.831 of invasion percolation with trapping (IPT) does not produce a data collapse. (d) For the largest MV_{0.8} cluster, we obtain a data collapse if $d_f = 2$.

Cluster sizes

The scaling laws for w and l signal that MV_{0.8} is not in the same universality class as IP. In Ref. [19] it is claimed that MV₁ is in yet another class, namely invasion percolation with trapping (IPT). Although w scales identically in IP and IPT [43], we now demonstrate how the gradient method can still show unequivocally that MV₁ belongs to the IP class after all, thus supporting the arguments of Ref. [22]. We calculate the size s_{\max} of the largest cluster in a lattice whose linear size is L in both x - and y -direction. We center the x -axis at p_c so that the initial probability to be black in Eq. 1 is limited by $\pm \frac{1}{2}gL + p_c$ on the right (left) edge. As a function of L and g , s_{\max} is expected to satisfy the ansatz

$$s_{\max} = L^{d_f} f_{s_{\max}}(L/\xi(g)). \quad (8)$$

Here d_f is the fractal dimension of the cluster at p_c , $\xi(g)$ is the characteristic length scale for changes in the cluster density, and the scaling function $f_{s_{\max}}(z)$ approaches a constant for $z \rightarrow 0^+$. The fractal dimensions differ between the two universality classes in question: $d_f = 91/48 \approx 1.896$ for IP and $d_f = 1.831(3)$ for IPT [44]. Furthermore, $\xi(g)$ in IP scales linearly with $w \propto g^{-4/7}$ [31]. Thus, according to Eq. 8, a plot of $s_{\max} L^{-91/48}$ versus $Lg^{4/7}$ collapses the IP data for different L and g on a single curve that asymptotically ap-

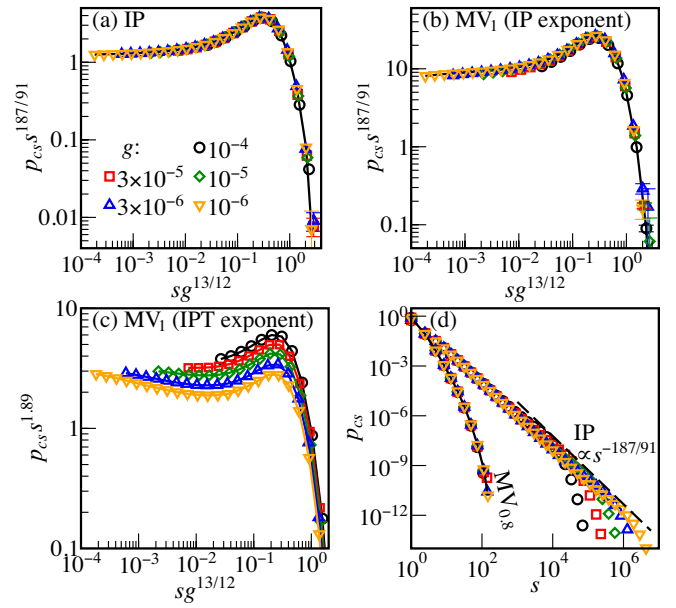


FIG. 4: **Cluster size distributions.** (a) The rescaled distribution $p_{cs} s^\tau$ for IP collapses if plotted versus $sg^{1/[\sigma(\nu+1)]}$, where the critical exponents ν , σ , τ are those of standard percolation. For MV₁ the data collapse is much better (b) for the IP exponent $\tau = 187/91$ than (c) for the IPT exponent $\tau = 1.89$. (d) The MV_{0.8} distribution does not follow the same asymptotic power law as IP.

proaches a constant for small $Lg^{4/7}$ (Fig. 3a). For MV₁, we obtain a data collapse with the same IP exponents (Fig. 3b). By contrast, if we assume $d_f = 1.831$, there is neither a collapse nor do the individual curves approach a constant for $Lg^{4/7} \rightarrow 0^+$ (Fig. 3c), hence ruling out that MV₁ is in the same universality class as IPT. Changing the exponent 4/7 on g leads to a lateral shift of the data in Fig. 3(c), but we found no value yielding a convincing data collapse. Moreover, it cannot overcome the problem that the hypothetical scaling function $f_{s_{\max}}(z)$ would not become constant for $z \rightarrow 0^+$. However, the collapse of MV_{0.8} with $d_f = 2$ (which justifies the solid-on-solid approximation in the previous section) and $\xi(g) \propto g^{-1}$ in Fig. 3(d) corroborates that opinion dynamics can lead to percolation outside the IP universality class.

The cluster size distribution provides further support for this classification. We count all non-spanning clusters with at least one site in the stripe $|x| < w$ and compute the fraction $p_{cs}(s)$ of clusters of size s . In IP [42]

$$p_{cs}(s) = s^{-\tau} f_{cs} \left(sg^{1/[\sigma(\nu+1)]} \right), \quad (9)$$

where the critical exponents are $\tau = 187/91 \approx 2.055$, $\sigma = 36/91$, $\nu = 4/3$ [45], and $f_{cs}(z) \rightarrow \text{const.}$ for $z \rightarrow 0^+$ (Fig. 4a). Reference [19] hypothesizes that in MV₁ the exponent τ is replaced by 1.89(1), the corresponding value for the pore size distribution in IPT. However, Fig. 4(b) and (c) show that, while the data collapse

is excellent for $\tau = 187/91$, it is poor for the alternative value 1.89. In summary, MV_1 and IP share the following critical exponents: the hull width and length exponents a , b and consequently $\nu = 4/3$; the fractal dimension d_f and thus $\beta = \nu(2 - d_f)$; furthermore τ and σ . This list is clear evidence that MV_1 is in the IP universality class. As shown in Appendix 4, we reach the same conclusion for UR_1 and $UR_{0.8}$.

The situation is different in $MV_{0.8}$ where the cluster size distribution appears to drop more sharply with a cutoff that varies much less with the gradient. We want to assess the lack of scaling quantitatively and distinguish it from a power law with large exponent τ and little dependence of the upper cutoff on g . Moment ratios $s_c^{(n)} = \langle s^{n+1} \rangle / \langle s^n \rangle$ are asymptotically proportional to the upper cutoff, provided $n > \tau - 1$. If the transition is continuous, then $s_c^{(n)}$ scales asymptotically as a power of g . This power law can be detected more easily than the asymptotic scaling regime $p_{cs} \propto s^{-\tau}$ [46].

We plot the moment ratios of IP, UR_1 , MV_1 , $UR_{0.8}$ and $MV_{0.8}$ for $n = 2, 3, 4$ in Fig. 5. Except $MV_{0.8}$, all of these cases are in excellent agreement with the prediction of Eq. 9, $s_c^{(n)} \propto g^{-1/[\sigma(\nu+1)]}$, where $\sigma = 36/91$ and $\nu = 4/3$ are the critical exponents of IP [45]. The cutoff $s_c^{(n)}$ in $MV_{0.8}$, by contrast, does not diverge as a power law for $g \rightarrow 0^+$. Instead $s_c^{(n)}$ appears to reach an asymptotic value for all n . Such a behavior is typical of a first-order transition. Based on these data, we can firmly rule out that τ in $MV_{0.8}$ has the IP value $187/91 \approx 2.055$. We add the caveat that, for sufficiently large n , $s_c^{(n)}$ may scale as a power of g after all. However, the data imply $\tau > 5$, an unusually large value compared to IP, directed percolation ($\tau = 2.112$) [47] and Achlioptas percolation ($\tau = 2.04762$) [48].

Conclusion

We have studied in total five opinion dynamics models on a gradient, as summarized in Table I. One of the models we studied, independent percolation, provides the very definition of the corresponding universality class, IP. We find that of the four other models studied, three display features that are fully compatible with IP, which is commonly observed in gradient models with and without interaction [29, 49, 50].

One model, $MV_{0.8}$, differs from all of the above. At $p = 1/2$ it has states with either a black or white majority. Without a gradient, (i.e. $g = 0$ in Eq. 1, so that $p(x) = 1/2$ is constant in x), there are two stable stationary solutions, where one state is above and the other

below the threshold of percolation of, say, black sites. There is hysteresis if one tries to move from one majority to the other by tuning p , as expected for first-order transitions. By introducing a gradient, the two phases are forced to collide because the left boundary must be completely white and the right boundary black. We observe that the gradient stabilizes and sharpens the front compared to independent percolation.

$MV_{0.8}$ differs from the other models in two important points. First, its stochastic nature helps anneal boundaries between opposite opinions. The second difference is that the majority rule makes small clusters more prone to invasion by the opposing opinion. The combination of these two features results in what appears to be a first-order transition. Nevertheless, the opinion interface displays scaling, found to be in the Edwards-Wilkinson universality class, which differs significantly from independent percolation.

The birth-death model of Ref. [42] suggested already the possibility of first-order transitions in gradient models. We leave it to future research to analytically confirm the first-order nature of the $MV_{0.8}$ transition. It would also be insightful to investigate more complex network topologies that are based on real social interactions rather than a regular square lattice. We emphasize that, in the light of previous work on explosive percolation [48, 51–53], only analytic results can fully clarify the order of any percolation transition. However, we can conclude with certainty that, although none of the opinion models we have investigated is consistent with IPT, $MV_{0.8}$ is an example of a dynamic rule that leads to percolation outside the IP universality class.

From a sociological perspective, our study shows that small variations in the innate propensity towards one or another opinion may turn into a spatial discontinuity in the opinions. Interestingly, the sharpest division occurs when agents do not follow the local majority all the time. Hence, processes that may be perceived as having the effect of making the interface between different opinions more blurred, such as the majority rule with stochasticity involved, have the opposite effect. They anneal this interface and contribute to the collapse of minority clusters, which are sustained in the presence of stricter rules, such as the deterministic unanimity rule.

Acknowledgments

MTG acknowledges support by Imperial College London and the European Commission (project number FP7-PEOPLE-2012-IEF 6-4564/2013).

[1] de Oliveira MJ (1992) Isotropic majority-vote model on a square lattice. *J Stat Phys* 66: 273–281.

[2] Sznajd-Weron K, Sznajd J (2000) Opinion evolution in closed community. *Int J Mod Phys C* 11: 1157.

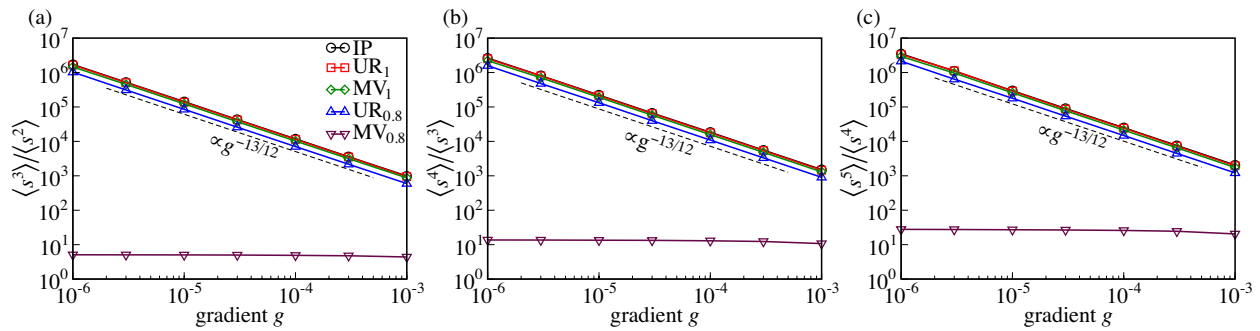


FIG. 5: **Cluster size moment ratios.** The moment ratios $\langle s^{n+1} \rangle / \langle s^n \rangle$ of the cluster size distributions for (a) $n = 2$, (b) $n = 3$, (c) $n = 4$. The ratios for UR₁, MV₁, and UR_{0.8} scale in the same manner as in IP, namely $\langle s^{n+1} \rangle / \langle s^n \rangle \propto g^{13/12}$. By contrast, the moment ratios for MV_{0.8} appear to reach an asymptotic limit for $g \rightarrow 0^+$.

Model	q	Exponents	Universality Class
Independent Percolation (IP)		$a = 4/7, b = 3/7, d_f = 91/48, \nu = 4/3$	IP (by definition)
Deterministic Majority Vote Model (MV ₁)	1	$a = 4/7, b = 3/7, d_f = 91/48, \nu = 4/3$	IP
Deterministic Unanimity Rule (UR ₁)	1	$a = 4/7, b = 3/7, d_f = 91/48, \nu = 4/3$	IP
Stochastic Majority Vote Model (MV _{0.8})	0.8	$a = 1/4, b = 0, d_f = 2$	Edwards-Wilkinson
Stochastic Unanimity Rule (UR _{0.8})	0.8	$a = 4/7, b = 3/7, d_f = 91/48, \nu = 4/3$	IP

TABLE I: Summary of the results. For definitions of models and exponents see text.

- [3] Krapivsky PL, Redner S (2003) Dynamics of majority rule in two-state interacting spins systems. Phys Rev Lett 90: 238701.
- [4] Galam S (2005) Local dynamics vs. social mechanisms: A unifying frame. Europhys Lett 70: 705-711.
- [5] Lambiotte R, Redner S (2007) Dynamics of vacillating voters. J Stat Mech 2007: L10001.
- [6] Roca C, Draief M, Helbing D (2012) Coordination and competitive innovation spreading in social networks. In: Helbing D, editor, Social Self-Organization, Berlin: Springer. pp. 169-184.
- [7] Castellano C, Fortunato S, Loreto V (2009) Statistical physics of social dynamics. Rev Mod Phys 81: 591-646.
- [8] Stauffer D (2013) A biased review of sociophysics. J Stat Phys 151: 9-20.
- [9] Moussaïd M, Kämmer JE, Analytis PP, Neth H (2013) Social influence and the collective dynamics of opinion formation. PLoS One 8: e78433.
- [10] Bernardes AT, Stauffer D, Kertész J (2002) Election results and the Sznajd model on Barabasi network. Eur Phys J B 25: 123-127.
- [11] González MC, Sousa AO, Herrmann HJ (2004) Opinion formation on a deterministic pseudo-fractal network. Int J Mod Phys C 15: 45-58.
- [12] Amini H, Draief M, Lelarge M (2009) Marketing in a random network. In: Altman E, Chaintreau A, editors, Network Control and Optimization, Berlin: Springer. pp. 17-25.
- [13] Martins ACR, de B Pereira C, Vicente R (2009) An opinion dynamics model for the diffusion of innovations. Physica A 388: 3225-3232.
- [14] Gradowski TM, Kosiński RA (2006) The effect of an electoral campaign for election results in an open community. Int J Mod Phys C 17: 1327-1338.
- [15] Watts DJ, Dodds PS (2007) Influentials, networks, and public opinion formation. J Consum Res 34: 441-458.
- [16] Liggett TM (1999) Stochastic Interacting Systems: Contact, Voter and Exclusion Processes. Berlin: Springer. 335 p.
- [17] Klinkner PA (2004) Red and blue scare: The continuing diversity of the American electoral landscape. The Forum 2: 2.
- [18] Stauffer D (2004) Difficulty for consensus in simultaneous opinion formation of Sznajd model. J Math Sociol 28: 25-33.
- [19] Shao J, Havlin S, Stanley HE (2009) Dynamic opinion model and invasion percolation. Phys Rev Lett 103: 018701.
- [20] Camia F, Newman CM, Sidoravicius V (2004) A particular bit of universality: Scaling limits of some dependent percolation models. Commun Math Phys 246: 311-332.
- [21] Shao J, Havlin S, Stanley HE (2012) Shao, Havlin, and Stanley reply. Phys Rev Lett 109: 079802.
- [22] Sattari A, Paczuski M, Grassberger P (2012) Comment on dynamic opinion model and invasion percolation. Phys Rev Lett 109: 079801.
- [23] Stauffer D, Sá Martins JS (2004) Simulation of Galam's contrarian opinions on percolative lattices. Physica A 334: 558-565.
- [24] Centola D, Willer R, Macy M (2005) The emperor's dilemma: A computational model of self-enforcing norms. Am J Sociol 110: 1009-1040.

- [25] Mobilia M, Petersen A, Redner S (2007) On the role of zealotry in the voter model. *J Stat Mech* 2007: P08029.
- [26] Cutler F, Jenkins RW (2002) Where one lives and what one thinks: Implications of rural-urban opinion cleavages for Canadian federalism. In: Lazar H, Telford H, editors, Canada: The State of the Federation 2001, Montreal: McGill-Queen's University Press. pp. 367–392.
- [27] Clem RS, Chodakiewicz MJ (2004) Poland divided: Spatial differences in the June 2003 EU accession referendum. *Eurasian Geogr Econ* 45: 475–490.
- [28] Lang R, Sanchez T, Berube A (2008) The new suburban politics: A county-based analysis of metropolitan voting trends since 2000. In: Teixeira R, editor, Red, Blue, and Purple America: The Future of Election Demographics, Washington: Brookings Institution Press. pp. 25–49.
- [29] Gouyet JF, Rosso M (2005) Diffusion fronts and gradient percolation: A survey. *Physica A* 357: 86–96.
- [30] Lambiotte R, Thurner S, Hanel R (2007) Unanimity rule on networks. *Phys Rev E* 76: 046101.
- [31] Sapoval B, Rosso M, Gouyet JF (1985) The fractal nature of a diffusion front and the relation to percolation. *J Physique Lett* 46: L149–L156.
- [32] Voss RF (1984) The fractal dimension of percolation cluster hulls. *J Phys A: Math Gen* 17: L373–L377.
- [33] Grossman T, Aharony A (1986) Structure and perimeters of percolation clusters. *J Phys A: Math Gen* 19: L745–L751.
- [34] Gastner MT, Oborny B, Zimmermann DK, Pruessner G (2009) Transition from connected to fragmented vegetation across an environmental gradient: Scaling laws in ecotone geometry. *Am Nat* 174: E23–E39.
- [35] Newman MEJ, Ziff RM (2000) Efficient Monte Carlo algorithm and high-precision results for percolation. *Phys Rev Lett* 85: 4104–4107.
- [36] Nolin P (2008) Critical exponents of planar gradient percolation. *Ann Probab* 36: 1748–1776.
- [37] Gastner MT, Oborny B (2012) The geometry of percolation fronts in two-dimensional lattices with spatially varying densities. *New J Phys* 14: 103019.
- [38] Vvedensky DD (2003) Edwards-Wilkinson equation from lattice transition rules. *Phys Rev E* 67: 025102(R).
- [39] Edwards SF, Wilkinson DR (1982) The surface statistics of a granular aggregate. *Proc R Soc Lond A* 381: 17–31.
- [40] Uhlenbeck GE, Ornstein LS (1930) On the theory of the Brownian motion. *Phys Rev* 36: 823.
- [41] Van Kampen NG (1992) *Stochastic Processes in Physics and Chemistry*. Amsterdam: Elsevier. 480 p.
- [42] Gastner MT, Oborny B, Ryabov AB, Blasius B (2011) Changes in the gradient percolation transition caused by an Allee effect. *Phys Rev Lett* 106: 128103.
- [43] Birovljev A, Furuberg L, Feder J, Jøssang T, Måløy KJ, et al. (1991) Gravity invasion percolation in two dimensions: Experiment and simulation. *Phys Rev Lett* 67: 584–587.
- [44] Schwarzer S, Havlin S, Bunde A (1999) Structural properties of invasion percolation with and without trapping: Shortest path and distributions. *Phys Rev E* 59: 3262–3269.
- [45] Stauffer D, Aharony A (1991) *Introduction to percolation theory*. London: Taylor & Francis, 2nd edition. 192 p.
- [46] Christensen K, Farid N, Pruessner G, Stapleton M (2008) On the scaling of probability density functions with apparent power-law exponents less than unity. *Eur Phys J B* 62: 331–336.
- [47] Dhar D, Barma M (1981) Monte Carlo simulation of directed percolation on a square lattice. *J Phys C: Solid State Phys* 14: L1–L6.
- [48] da Costa RA, Dorogovtsev SN, Goltsev AV, Mendes JFF (2010) Explosive percolation transition is actually continuous. *Phys Rev Lett* 105: 255701.
- [49] Gouyet JF (1988) Structure of diffusion fronts in systems of interacting particles. *Solid State Ionics* 28–30: 72–81.
- [50] Hader A, Memsouk A, Boughaleb Y (2002) Universality in diffusion front growth dynamics. *Eur Phys J B* 28: 315–319.
- [51] Achlioptas D, D'Souza RM, Spencer J (2009) Explosive percolation in random networks. *Science* 323: 1453–1355.
- [52] Riordan O, Warnke L (2011) Explosive percolation is continuous. *Science* 333: 322–324.
- [53] Cho YS, Hwang S, Herrmann HJ, Kahng B (2013) Avoiding a spanning cluster in percolation models. *Science* 339: 1185–1187.
- [54] Kroll DM (1981) Solid-on-solid model for the interface pinning transition in Ising ferromagnets. *Z Phys B* 41: 345–348.

Appendix 1: Transition probabilities in the hull dynamics of the majority vote model (Eq. 3–5)

Let the hull be parameterized as $(x_1, y_1), \dots, (x_l, y_l)$ by the left-turning walk described above at the end of the Methods section. Figure 1c shows that the hull in $MV_{0.8}$ separates a predominantly white region on the left from a similarly dense black region on the right. This observation justifies a “solid-on-solid” approximation [54] where we ignore

- any overhangs in the interface (i.e., parts of the left-turning walk that move towards smaller y -coordinates),
- any isolated islands of the minority color to the left and right of the hull.

In this approximation, the hull at time step t is completely characterized by

$$h(t, y) = \min\{x_k | y_k = y, k = 1, \dots, l\} - \frac{1}{2} \quad (10)$$

because every site (x, y) with $x < h(t, y)$ will be white and every site with $x > h(t, y)$ black. We now have to distinguish three cases.

Case 1: $h(t, y)$ is neither a strict local minimum nor maximum

In this case, one of the following four conditions must be met

- $h(t, y - 1) = h(t, y)$,
- $h(t, y) = h(t, y + 1)$,

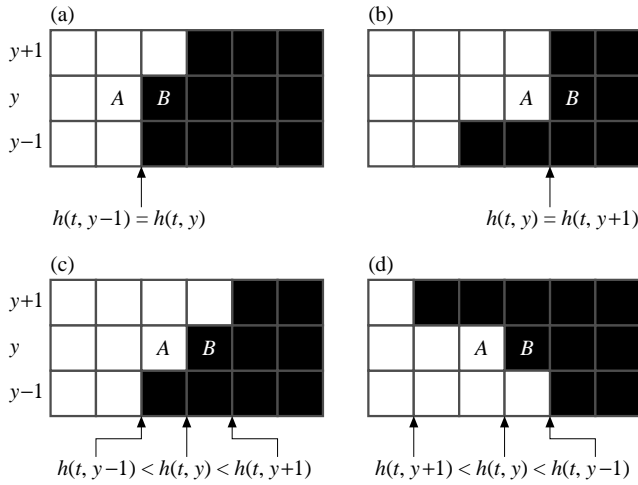


FIG. 6: Examples where $h(t, y)$ is neither a strict local minimum nor maximum. In each case, the white and black sites at the interface, A and B , have at least two neighbors of their own color so that in MV_1 there is no change of the hull position (i.e., $h(t, y) = h(t+1, y)$). In MV_{1-r} , there is a $O(r)$ probability that the hull moves one site to the left or right. All other probabilities are $O(r^2)$.

- $h(t, y-1) < h(t, y) < h(t, y+1)$, or
- $h(t, y-1) > h(t, y) > h(t, y+1)$.

Let A be the white site in the y -th row with x -coordinate $h(t, y) - \frac{1}{2}$ and B the black site at $h(t, y) + \frac{1}{2}$ (see Fig. 6). In all cases listed above, both A and B have at least two neighbors of their own color, namely one in the y -th row and one in a neighboring row. Including their own vote, the local majority supports their current opinion. As a consequence, in the deterministic majority vote model MV_1 neither A nor B will change color and thus $h(t+1, y) = h(t, y)$. In the stochastic model MV_{1-r} with $r > 0$, the probability that A becomes black is

$$\Pr[A \text{ black at } t+1 \mid h(t, y) = x] = r \left[g \left(x - \frac{1}{2} \right) + p_c \right], \quad (11)$$

and the probability that B becomes white

$$\Pr[B \text{ white at } t+1 \mid h(t, y) = x] = r \left[1 - g \left(x + \frac{1}{2} \right) - p_c \right]. \quad (12)$$

In the solid-on-solid approximation, the hull can shift exactly one step to the left only if A turns black, while all other sites keep their colors with a probability $1 - O(r)$. Because the probabilities are independent, we can multiply them and obtain

$$\Pr[h(t+1, y) = x-1 \mid h(t, y) = x] = r \left[g \left(x - \frac{1}{2} \right) + p_c \right] + O(r^2). \quad (13)$$

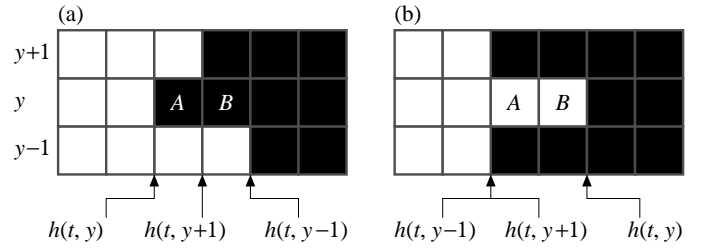


FIG. 7: Examples where $h(t, y)$ is a strict local (a) minimum or (b) maximum. The minimal or maximal site of the protruding opinion is in a local minority, but all other sites in row y will have at least two neighbors of the same opinion. Thus, in MV_1 only the front site will change opinion between time steps t and $t+1$. In MV_{1-r} the probability of the hull shifting one step towards the (a) right, (b) left is $1 - O(r)$. The probability of no change or two steps to the (a) right, (b) left is $O(r)$. All other transitions have probabilities $O(r^2)$.

Similarly,

$$\Pr[h(t+1, y) = x+1 \mid h(t, y) = x] = r \left[1 - g \left(x + \frac{1}{2} \right) - p_c \right] + O(r^2). \quad (14)$$

Because shifts of more than one step to either side have probabilities $O(r^2)$ and the sum of the probabilities must equal one,

$$\Pr[h(t+1, y) = x \mid h(t, y) = x] = 1 + r(g-1) + O(r^2). \quad (15)$$

Case 2: $h(t, y)$ is a strict local minimum

Here the leftmost black site A in row y is in a local minority (see Fig. 7a). It stays black with probability

$$\Pr[A \text{ black at } t+1 \mid h(t, y) = x] = r \left[g \left(x + \frac{1}{2} \right) + p_c \right]. \quad (16)$$

Its right neighbor B is black, which is the local majority because at least its two neighbors in row i are black. Hence, it becomes white with probability

$$\Pr[B \text{ white at } t+1 \mid h(t, y) = x] = r \left[1 - g \left(x + \frac{3}{2} \right) - p_c \right]. \quad (17)$$

In the solid-on-solid approximation, the hull can only stay at the same position if none of the sites in row i changes its color. With the only exception of A , an individual opinion change has probability $1 - O(r)$ for all sites so that

$$\Pr[h(t+1, y) = x \mid h(t, y) = x] = r \left[g \left(x + \frac{1}{2} \right) + p_c \right] + O(r^2). \quad (18)$$

The hull can only shift two sites to the right if A and B become white. The former has probability $1 - O(r)$, the latter is given by Eq. 17, and all other probabilities are $1 - O(r)$. Therefore,

$$\Pr[h(t+1, y) = x+2 | h(t, y) = x] = r \left[1 - g \left(x + \frac{3}{2} \right) - p_c \right] + O(r^2). \quad (19)$$

All other shifts further to the left and right are $O(r^2)$, so that the only remaining transition of one step to the right has probability

$$\Pr[h(t+1, y) = x+1 | h(t, y) = x] = 1 + r(g-1) + O(r^2). \quad (20)$$

Case 3: $h(t, y)$ is a strict local maximum

In analogy to case 2, we find

$$\Pr[h(t+1, y) = x | h(t, y) = x] = r \left[1 - g \left(x - \frac{1}{2} \right) - p_c \right] + O(r^2), \quad (21)$$

$$\Pr[h(t+1, y) = x-2 | h(t, y) = x] = r \left[g \left(x - \frac{3}{2} \right) + p_c \right] + O(r^2), \quad (22)$$

$$\Pr[h(t+1, y) = x-1 | h(t, y) = x] = 1 + r(g-1) + O(r^2). \quad (23)$$

Summary

We can summarize the results so far with the notation

$$K_y = \begin{cases} +1 & \text{if } h(t, y) \text{ is a strict minimum,} \\ -1 & \text{if } h(t, y) \text{ is a strict maximum,} \\ 0 & \text{otherwise.} \end{cases} \quad (24)$$

Neglecting terms $O(r^2)$,

$$\Pr[h(t+1, y) = x-1 + K_y | h(t, y) = x] = r \left[g \left(x - \frac{1}{2} \right) + p_c \right] + r g K_y, \quad (25)$$

$$\Pr[h(t+1, y) = x + K_y | h(t, y) = x] = 1 + r(g-1), \quad (26)$$

$$\Pr[h(t+1, y) = x+1 + K_y | h(t, y) = x] = r \left[1 - g \left(x + \frac{1}{2} \right) - p_c \right] - r g K_y. \quad (27)$$

Because there are no isolated clusters in the solid-on-solid approximation and the dynamics is symmetric under interchange of black and white, p_c equals $\frac{1}{2}$. This assumption is consistent with our numerical results for the full model $p_c = 0.5000(4)$. Equations 25–27 with $p_c = \frac{1}{2}$ yield Eq. 3–5.

Appendix 2: The stochastic differential equation for the hull evolution (Eq. 6)

An alternative formulation of Eq. 25–27 is

$$h(t+1, y) = h(t, y) + K_y + \zeta_y, \quad (28)$$

where

$$\Pr(\zeta_y = -1) = r \left[\frac{1}{2} + g \left(h(t, y) - \frac{1}{2} + K_y \right) \right], \quad (29)$$

$$\Pr(\zeta_y = 0) = 1 + r(g-1), \quad (30)$$

$$\Pr(\zeta_y = 1) = r \left[\frac{1}{2} - g \left(h(t, y) + \frac{1}{2} + K_y \right) \right]. \quad (31)$$

The expectation value of ζ_y is

$$\langle \zeta_y \rangle = -2gr(h + K_y), \quad (32)$$

so that we can rephrase Eq. 28 as

$$\underbrace{h(t+1, y) - h(t, y)}_A = \underbrace{K_y - 2gr(h + K_y)}_B + \underbrace{\zeta_y - \langle \zeta_y \rangle}_C. \quad (33)$$

Our objective is to take the continuum limit of Eq. 33 in the following manner. With the notation

$$\Delta_+ = h(t, y+1) - h(t, y), \quad (34)$$

$$\Delta_- = h(t, y) - h(t, y-1), \quad (35)$$

we can express K_y of Eq. 24 using the Heaviside step function

$$\theta(x) = \begin{cases} 1 & \text{if } x \geq 0, \\ 0 & \text{otherwise} \end{cases} \quad (36)$$

as

$$K_y = [1 - \theta(-\Delta_+)] [1 - \theta(\Delta_-)] - [1 - \theta(\Delta_+)] [1 - \theta(-\Delta_-)]. \quad (37)$$

The discontinuous Heaviside function can be written as the limit $\epsilon \rightarrow 0$ of the differentiable function [38]

$$\theta_\epsilon(x) = \epsilon \ln \left(\frac{\exp\left(\frac{x+1}{\epsilon}\right) + 1}{\exp\left(\frac{x}{\epsilon}\right) + 1} \right). \quad (38)$$

Simultaneously with the limit of the Heaviside function, we take the continuum limit of the space and time variables,

$$\tilde{t} = \epsilon^k t, \quad (39)$$

$$\tilde{y} = \epsilon^l y, \quad (40)$$

$$\tilde{h}(\tilde{t}, \tilde{y}) = \epsilon^m h(t, y), \quad (41)$$

with $k, l, m > 0$ and let g approach zero as

$$g = \epsilon^n \tilde{g} \quad (42)$$

with $n > 0$. We will now determine the leading terms in the individual parts of Eq. 33, which will give us conditions for these exponents.

I: The discrete time derivative A in Eq. 33

$$\frac{d\theta_\epsilon(0)}{dx} = \frac{1}{2} + O\left(e^{-1/\epsilon}\right), \quad (45)$$

Assuming that h is a smooth function, we can expand A as

$$\begin{aligned} A &= \epsilon^{-m} \left(\tilde{h}(\tilde{t} + \epsilon^k) + \tilde{h}(\tilde{t}) \right) \\ &= \epsilon^{k-m} \frac{\partial \tilde{h}}{\partial \tilde{t}} + O\left(\epsilon^{2k-m}\right). \end{aligned} \quad (43)$$

$$\frac{d^2\theta_\epsilon(0)}{dx^2} = -\frac{1}{4\epsilon} + O\left(\epsilon^{-1}e^{-1/\epsilon}\right), \quad (46)$$

II: The variable K_y encoding a strict minimum or maximum

For the derivatives of θ_ϵ of Eq. 38, we find

$$\theta_\epsilon(0) = 1 - \epsilon \ln(2) + O\left(\epsilon e^{-1/\epsilon}\right), \quad (44)$$

$$\frac{d^3\theta_\epsilon(0)}{dx^3} = O\left(\epsilon^{-2}e^{-1/\epsilon}\right). \quad (47)$$

Inserting these derivatives into Eq. 37 we obtain

$$\begin{aligned} K_{y,\epsilon} &= \left[\epsilon \ln(2) + \frac{1}{2}\Delta_+ - \frac{1}{8\epsilon}\Delta_+^2 + O\left(\epsilon^{-3}\Delta_+^4\right) \right] \left[\epsilon \ln(2) - \frac{1}{2}\Delta_- - \frac{1}{8\epsilon}\Delta_-^2 + O\left(\epsilon^{-3}\Delta_-^4\right) \right] \\ &\quad - \left[\epsilon \ln(2) + \frac{1}{2}\Delta_- - \frac{1}{8\epsilon}\Delta_-^2 + O\left(\epsilon^{-3}\Delta_-^4\right) \right] \left[\epsilon \ln(2) - \frac{1}{2}\Delta_+ - \frac{1}{8\epsilon}\Delta_+^2 + O\left(\epsilon^{-3}\Delta_+^4\right) \right] \\ &= \epsilon \ln(2) (\Delta_+ - \Delta_-) + \frac{1}{8\epsilon}\Delta_+\Delta_-(\Delta_+ - \Delta_-) + O\left(\epsilon^{-3}\Delta^5\right). \end{aligned} \quad (48)$$

From the Taylor expansions of \tilde{h} we obtain

$$\Delta_+ - \Delta_- = \epsilon^{2l-m} \frac{\partial^2 \tilde{h}}{\partial \tilde{y}^2} + O\left(\epsilon^{4l-m}\right), \quad (49)$$

$$\begin{aligned} \Delta_+\Delta_-(\Delta_+ - \Delta_-) &= \\ \epsilon^{4l-3m} \left(\frac{\partial \tilde{h}}{\partial \tilde{y}} \right)^2 \frac{\partial^2 \tilde{h}}{\partial \tilde{y}^2} &+ O\left(\epsilon^{6l-3m}\right), \end{aligned} \quad (50)$$

so that

$$K_{y,\epsilon} = \epsilon^{2l-m+1} \ln(2) \frac{\partial^2 \tilde{h}}{\partial \tilde{y}^2} + O\left(\epsilon^{4l-3m-1}\right), \quad (51)$$

where the expansion converges only if

$$l - m > 1. \quad (52)$$

III: The gradient term B in Eq. 33

From Eq. 41, 42 and 51, we obtain

$$\begin{aligned} B &= 2\epsilon^n \tilde{g}r \left[\epsilon^{-m} \tilde{h}(\tilde{t}, \tilde{y}) + O\left(\epsilon^{2l-m+1}\right) \right] \\ &= 2\epsilon^{n-m} \tilde{g}r \tilde{h}(\tilde{t}, \tilde{y}) + O\left(\epsilon^{2l-m+n+1}\right). \end{aligned} \quad (53)$$

IV: The noise term C in Eq. 33

The covariance of the noise is

$$\begin{aligned} \left\langle [\zeta_y(t) - \langle \zeta_y(t) \rangle] \times [\zeta_{y'}(t') - \langle \zeta_{y'}(t') \rangle] \right\rangle &= \\ [r(1-g) + O(r^2)] \delta_{t,t'} \delta_{y,y'}. \end{aligned} \quad (54)$$

In the continuum limit, the Kronecker deltas transform as

$$\delta_{t,t'} = \epsilon^k \delta(\tilde{t} - \tilde{t}'), \quad (55)$$

$$\delta_{y,y'} = \epsilon^l \delta(\tilde{y} - \tilde{y}'). \quad (56)$$

Dropping terms of order $O(r^2)$,

$$\begin{aligned} \langle C(\tilde{t}, \tilde{y}) C(\tilde{t}', \tilde{y}') \rangle &= \\ \epsilon^{k+l} r \delta(\tilde{t} - \tilde{t}') \delta(\tilde{y} - \tilde{y}') &+ O\left(\epsilon^{k+l+n}\right), \end{aligned} \quad (57)$$

where $C(\tilde{t}, \tilde{y}) = \zeta_{\tilde{y}}(\tilde{t}) - \langle \zeta_{\tilde{y}}(\tilde{t}) \rangle$ is defined as in Eq. 33. If we introduce the rescaled noise

$$\eta(\tilde{t}, \tilde{y}) = \frac{\epsilon^{-(k+l)/2}}{\sqrt{r}} C(\tilde{t}, \tilde{y}), \quad (58)$$

then the covariance

$$\langle \eta(\tilde{t}, \tilde{y}) \eta(\tilde{t}', \tilde{y}') \rangle = \delta(\tilde{t} - \tilde{t}') \delta(\tilde{y} - \tilde{y}') + O(\epsilon^n) \quad (59)$$

is to highest order independent of ϵ .

V: Summary

Including only the leading terms, Eq. 33 becomes

$$\epsilon^{k-m} \frac{\partial \tilde{h}}{\partial \tilde{t}} = \epsilon^{2l-m+1} \ln(2) \frac{\partial^2 \tilde{h}}{\partial \tilde{y}^2} - 2\epsilon^{n-m} \tilde{g} r \tilde{h}(\tilde{t}, \tilde{y}) + \sqrt{r} \epsilon^{(k+l)/2} \eta(\tilde{t}, \tilde{y}). \quad (60)$$

The four different terms scale with the same power of ϵ if

$$l = \frac{1}{2}(k-1), \quad (61)$$

$$m = \frac{1}{4}(k+1), \quad (62)$$

$$n = k. \quad (63)$$

The inequality of Eq. 52 can be satisfied by $k > 7$. Dividing Eq. 60 by $\epsilon^{k-m} = \epsilon^{2l-m+1} = \epsilon^{n-m} = \epsilon^{(k+l)/2}$ yields Eq. 6.

Appendix 3: The derivation of the hull width (Eq. 7)

We consider Eq. 6 with periodic boundaries at $y = 0$ and $y = L$. The solution $G(t, y)$ of the deterministic

equation

$$\frac{\partial G}{\partial t} = D \frac{\partial^2 G}{\partial y^2} - EgG \quad (64)$$

with initial condition $\lim_{t \rightarrow 0} G(t, y) = \delta(y - y_0)$ is

$$G(t, y; y_0) = \frac{1}{L} \sum_{n=-\infty}^{\infty} \exp[-(Dk_n^2 + Eg)t + ik_n(y - y_0)], \quad (65)$$

where $k_n = 2\pi n/L$. The hull position can be expressed in terms of G as

$$h(t, y) = F \int_0^L dy_0 \int_0^t dt' G(t - t', y; y_0) \eta(t', y_0). \quad (66)$$

Combining the last two expressions, we can derive

$$\langle h(t, y) h(t, y') \rangle = \frac{F^2}{2L} \sum_{n=-\infty}^{\infty} \frac{1 - \exp(-2(Dk_n^2 + Eg)t)}{Dk_n^2 + Eg} \exp[ik_n(y' - y)] \quad (67)$$

The hull width is

$$w^2(L) = \lim_{t \rightarrow \infty} \left\langle \left(\frac{1}{L} \int_0^L dy h^2(t, y) - \left(\frac{1}{L} \int_0^L dy h(t, y) \right)^2 \right) \right\rangle = \frac{F^2}{L} \sum_{n=1}^{\infty} (Dk_n^2 + Eg)^{-1} = \frac{F^2}{2} \left(\frac{\coth\left(\frac{L}{2} \sqrt{\frac{Eg}{D}}\right)}{2\sqrt{DEg}} - \frac{1}{EgL} \right). \quad (68)$$

In the limit of large system size

$$\lim_{L \rightarrow \infty} w^2(L) = \frac{F^2}{4\sqrt{DEg}}, \quad (69)$$

which is identical with Eq. 7.

Appendix 4: UR₁ and UR_{0.8} are in the IP universality class

In Fig. 3 and 4 we show collapse plots for the maximum cluster size s_{\max} and the cluster size distribution p_{cs} for

IP and MV₁. In these cases, the data points lie on a single curve when we plot $s_{\max} L^{d_f}$ versus $Lg^{\nu/(\nu+1)}$ and $p_{cs} s^{-\tau}$ versus $sg^{1/[\sigma(\nu+1)]}$. The crucial observation is that the collapse occurs when inserting the IP critical exponents $d_f = 91/48$, $\nu = 4/3$, $\tau = 187/91$ and $\sigma = 36/91$ in these expressions, a telltale sign that MV₁ is indeed in the IP universality class.

In Fig. 8 we make the equivalent plots for UR_{0.8} and UR₁ with the same exponents. The data again fall on a single curve in each case. Moreover, we have already seen in Fig. 2 that for both of these models $w \propto g^{-\nu/(\nu+1)}$ and $b \propto g^{-1/(\nu+1)}$ as in IP. Thus, all numerical evidence

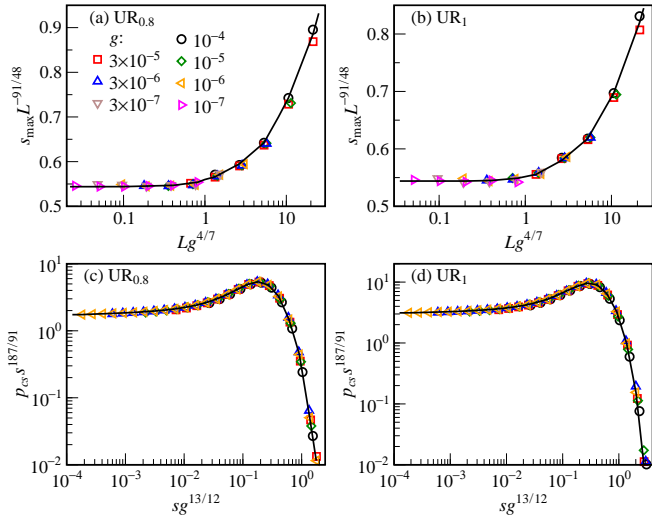


FIG. 8: Collapse plots for (a) the size of the largest cluster s_{\max} in $UR_{0.8}$, (b) in UR_1 , (c) the cluster size distribution p_{cs} for $UR_{0.8}$, (d) UR_1 .

points to both $UR_{0.8}$ and UR_1 (unlike $MV_{0.8}$) belonging to the IP universality class.